

Information-Theoretical Approach to Integrated Pulse-Doppler Radar and Communication Systems

Geon Choi and Namyoon Lee, *Senior Member, IEEE*

Abstract

Integrated sensing and communication improves the design of systems by combining sensing and communication functions for increased efficiency, accuracy, and cost savings. The optimal integration requires understanding the trade-off between sensing and communication, but this can be difficult due to the lack of unified performance metrics. In this paper, an information-theoretical approach is used to design the system with a unified metric. A sensing rate is introduced to measure the amount of information obtained by a pulse-Doppler radar system. An approximation and lower bound of the sensing rate is obtained in closed forms. Using both the derived sensing information and communication rates, the optimal bandwidth allocation strategy is found for maximizing the weighted sum of the spectral efficiency for sensing and communication. The simulation results confirm the validity of the approximation and the effectiveness of the proposed bandwidth allocation.

I. INTRODUCTION

The persistent trend of spectrum scarcity in wireless communications has prompted the development of Integrated Sensing and Communication (ISAC), a revolutionary approach to provide high-speed communication and precise sensing services within limited spectrum availability. Unlike traditional communication and sensing systems, which are independently designed with separate hardware platforms and orthogonal spectrums, ISAC optimizes the system by sharing bandwidth and hardware [1]–[5]. This joint design approach enhances spectral efficiency and sensing accuracy, while also reducing hardware costs. ISAC has gained popularity as a solution

G. Choi is with the Department of Electrical Engineering, POSTECH, South Korea, Pohang, (e-mail: simon03062@postech.ac.kr). N. Lee is with the School of Electrical Engineering, Korea University, South Korea, Seoul, (e-mail: namyoon@korea.ac.kr)

for emerging applications, including autonomous driving in vehicular networks, indoor positioning with WiFi signals, and joint radar imaging and communication systems [6]–[11].

The integration of sensing and communication systems presents a major challenge due to the lack of understanding of the trade-off between their performance when sharing the same radio spectrum. While the classical Shannon theory [12] outlines the limit of communication systems, it remains unclear what the maximum amount of reliable information can be obtained from unknown objects (e.g., distances, velocities, angle of arrivals, and reflected power levels) in a sensing system for a given time-frequency resource. Historically, radar systems have been designed to accurately estimate the features of unknown objects, with mean-squared error (MSE) [13] and Cramer-Rao lower bound (CRLB) [14] being popular performance metrics. However, the lack of a connection between Fisher information and mutual information in information theory impedes the design of integrated sensing and communication systems with a unified performance metric. Thus, a unified performance metric is crucial for optimal integration of these heterogeneous systems.

In this paper, we present a new metric, the *sensing rate*, for pulse-Doppler radar systems. The rate measures the amount of information about the target’s environment obtained from the radar’s returned signals. By using this rate, we derive the optimal bandwidth allocation strategy for ISAC systems that maximizes the combined spectral efficiency of both sensing and communication systems.

A. Related Work

There have been extensive efforts to evaluate information rates of a sensing system employing an information-theoretic approach. The pioneering work on incorporating the information-theoretical metric for sensing systems was found in [15]–[17]. The idea is to connect CRLB of the time delay estimation of a target to the differential entropy in measuring the target’s uncertainty. The estimation radar rate is defined as the amount of the change for differential entropies between a returned signal and the signal after applying radar post-processing for the delay estimation. Armed with this tool, a trade-off between sensing and communication rates was characterized in different resource-sharing scenarios. In analogy to [18], the radar rate was derived using the CRLB of a target location in multi-antenna sensing systems, and the trade-offs between radar and communication rates were derived in a multi-antenna ISAC setting. Very

recently, using the fact that CRLB constitutes a lower bound for the MSE of unbiased estimators [19], [20], the CLRB-rate region was derived to characterize the trade-off of ISAC systems.

An approach to understanding the information-theoretic limitation for an ISAC problem was initially introduced in [21], in which a transmitter sends a message to a receiver via a state-dependent stationary memoryless channel, and it estimates the state of the channel under the minimum distortion using a strictly causal channel output feedback. The trade-off between communication rates and state estimation accuracy in their setup was characterized using a capacity-distortion function. Recently, this approach has been extended to multi-user communication scenarios, including multiple access and broadcast channels in their subsequent works [22], [23]. In addition, the simultaneous binary state estimation and data communication problem was considered in [24] and characterized a trade-off in terms of communication rate against the error exponent in detecting the binary channel state.

Although these prior works have opened a new direction toward optimally integrating the sensing and communication systems from an information-theoretical viewpoint, these approaches still have limitations to understanding the sensing rate for widely-used pulse-Doppler radar systems (e.g., radar imaging applications). A pulse-Doppler radar is a sensing system that simultaneously determines a target's range, velocity, and reflected power by sending multiple pulses repeatedly during a coherent processing interval (CPI) [13], [25]–[27]. In a pulse-Doppler radar, the range and doppler resolutions are determined as a function of signal bandwidth and coherent processing interval (CPI), respectively. Instead of CRLB for the parameter estimation, these resolutions are more decisive because they limit the accuracy of the range and doppler estimation. Consequently, these parameters should be incorporated when defining the sensing rate. Unfortunately, all prior works in [15]–[24] do not consider these resolution effects when defining the sensing rates.

In a sensing system, a reflected signal by a target, referred to as a target signal, can be interpreted as *a transmitted signal by a target in environments*; thereby, it is essential to exploit the distribution of the target signal to measure the uncertainty of a target in a sensing system. The Swerling target models have been popularly used in radar systems, which combines a probability density function (PDF) and a decorrelation time for the target radar cross-section (RCS) [28]. For instance, In Swerling I and Swerling II target models, the total RCS is assumed to be the sum of many independent small scatterers, each with approximately equal individual RCS power in analogy to modeling a rich-scattering channel in communications. Furthermore, in Swerling

I, this total RCS is assumed to be constant during CPI, and the amplitude is distributed as Rayleigh in analogy to a block fading model in communications. In Swerling II, however, the total RCS is assumed to change with every pulse per scan, i.e., a fast-fading channel model in communications. As a result, unlike the previously defined sensing rates in [15]–[20], the sensing rate also requires incorporating the statistical distributions of the target signals.

B. Contributions

How much information rate is acquired by the pulse-Doppler radar system from targets in an environment? In this paper, we address this question by introducing a new concept - the sensing rate of a range-Doppler radar system. This rate is calculated as a combination of range, Doppler resolutions, and target's statistical distributions. Unlike previous works in [15]–[20] that utilize CRLB, our approach is based on more practical models and assumptions of the pulse-Doppler radar system. The key contributions of this paper are outlined below:

- We first introduce the concept of sensing rate, which quantifies the amount of information obtained from a target in terms of bits per channel use. We then derive the MSE-optimal target detector under the Bernoulli-Gaussian target distribution, demonstrating that it generalizes the traditional Neyman-Pearson detector. By utilizing the I-MMSE relationship from [29], we derive an exact expression for the sensing rate in integral form. This expression reveals that the sensing rate is comprised of two components, related to the target's location and fluctuation information. By leveraging this insight, we establish a connection between information-theoretic measures and estimation-theoretic measures, such as the minimum target detection error probability and the minimum MSE of target RCS.
- We also derive a tight approximation and a lower bound of the sensing rate in closed-form expressions that maintain full generality. These expressions are valuable in comprehending how the sensing rate varies based on system parameters. The derived lower bound of the sensing rate clearly indicates that the rate is directly proportional to the target uncertainty in the range-Doppler plane and the target signal-to-noise ratio (SNR). Our simulations validate the accuracy of the derived analytical expressions.
- To shed light on the derived sensing rate, we present an optimal bandwidth allocation strategy for an ISAC system. To the best of our knowledge, no prior studies have explored the optimal bandwidth allocation problem for an ISAC system that maximizes the weighted sum spectral efficiency, due to the lack of a definition of sensing rates in terms of bits

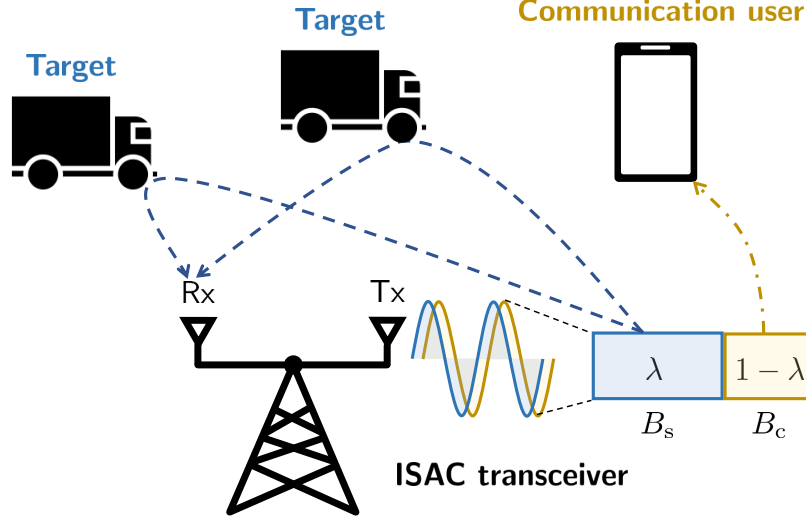


Fig. 1. An illustration of a ISAC system model.

per channel use. With the derived information sensing rate and Shannon's rate, our optimal bandwidth allocation strategy seeks to maximize the weighted sum spectral efficiency of both the sensing and communication rates. By deriving the first-order optimality condition for the weighted sum spectral efficiency, our strategy suggests that the ISAC system should allocate more bandwidth to the sensing system as the target uncertainty and signal power increase. This confirms our intuition, and simulation results show that our derived bandwidth allocation solution outperforms traditional uniform bandwidth allocation strategies.

II. SYSTEM MODEL

In this section, we present an ISAC system model. As illustrated in Fig. 1, an ISAC transceiver sends a pulse train and receives echoes for sensing an unknown environment. Meanwhile, it also transmits a message to a receiver for communications. The total system bandwidth is assumed to be B , and the sensing and communication systems use a fraction of the total bandwidth, i.e., $B_s = \lambda B$ and $B_c = (1 - \lambda)B$ for $\lambda \in [0, 1]$. We explain the signal models for the sensing system, and then define the performance metric for the ISAC system.

A. Pulse-Doppler Radar System Model

We first explain the continuous-time baseband signal models and the relevant assumptions for pulse-Doppler radar systems. Then, we present the equivalent discrete-time signal models for

pulse-Doppler radar systems when applying conventional radar post-processing.

1) *Continuous-time signal model*: The radar sends signal $x(t)$ comprised of M narrowband pulses $g(t)$ with pulse repetition interval (PRI) T_p during coherent processing interval (CPI) as

$$x(t) = \sum_{m=0}^{M-1} g(t - mT_p), \quad 0 \leq t \leq MT_p, \quad (1)$$

where the pulse $g(t)$ has the bandwidth of $B_s = 1/T_s$ and transmit energy $\int_0^{T_s} |g(t)|^2 dt = P_t T_s$. This transmitted signal is reflected by targets in an unknown environment.

We adopt the Swerling I target model [28]. This target model has been widely used to capture a static environmental scenario in the time scale of CPI. In this model, L non-fluctuating point targets are well-spread during CPI, and L targets are assumed to be statistically independent. Each target is defined by three parameters: i) range d_ℓ , ii) radial velocity v_ℓ , and iii) complex amplitude H_ℓ for $\ell \in [L]$. The range and the radial velocity of target ℓ correspond to round-trip time-delay $\tau_\ell = 2d_\ell/c$ and normalized doppler frequency $\nu_\ell = 2f_c v_\ell/c$. The complex amplitude H_ℓ is assumed to be drawn from IID complex Gaussian with mean $\mu_{T,\ell}$ and variance $\sigma_{T,\ell}^2$, i.e., $H_\ell \sim \mathcal{CN}(\mu_{T,\ell}, \sigma_{T,\ell}^2)$ for $\ell \in [L]$.

We assume that the radar system operates under the following target assumptions:

- Assumption 1: The target is static during CPI; this condition holds when the target delays $\{\tau_\ell\}_{\ell=1}^L$, Doppler frequencies $\{\nu_\ell\}_{\ell=1}^L$, and the complex amplitude $\{H_\ell\}_{\ell=1}^L$ are constant during CPI. In other words, the target state changes slowly in time and frequency.
- Assumption 2: The L delay-Doppler pairs $\{\tau_\ell, \nu_\ell\}_{\ell=1}^L$ are uniquely localized in the delay-Doppler plane defined by $[0, T_p] \times \left[-\frac{1}{2T_p}, \frac{1}{2T_p}\right]$. This fact implies that any two distinct targets cannot be overlapped in the plane, i.e., no ambiguity in the target presence.

Under the aforementioned assumptions, the continuous-time baseband received signal from the target reflections during CPI is given by

$$y(t) = \sum_{m=0}^{M-1} \sum_{\ell=1}^L \sqrt{\beta_\ell} H_\ell g(t - \tau_\ell - mT_p) e^{j2\pi m \nu_\ell t} + w(t), \quad (2)$$

where $w(t)$ is the complex additive white Gaussian noise with mean zero and variance $B_s N_0$, which is defined as the product of signal bandwidth B_s and noise spectral density N_0 . In addition, β_ℓ is the received signal power from the ℓ th target reflection, which is defined by the classical radar equation:

$$\beta_\ell = \frac{P_t G_t}{4\pi d_\ell^2} \frac{\sigma_{\text{rcs}} A_{\text{eff}}}{4\pi d_\ell^2}, \quad (3)$$

where $d_\ell = \tau_\ell c/2$ is the distance from the ℓ th target to the receiver, σ_{rcs} denotes the RCS of a target measured in m^2 , and A_{eff} is the effective area of the receiving antenna.

Let $x_m(t)$ be the noise-free received signal during the m th PRI, which is defined as

$$x_m(t) = \sum_{\ell=1}^L \sqrt{\beta_\ell} H_\ell g(t - \tau_\ell - mT_p) e^{-j2\pi m \nu_\ell T_p} \quad (4)$$

for $mT_p \leq t < (m+1)T_p$. This noise-free returned signal is of significance because it can be interpreted as the transmitted signal by the environment, i.e., a target signal. As a result, from a communication system perspective, the target signal plays the role of the transmitted signal by the targets. Using $x_m(t)$, we can rewrite the received signal in (2) during the m th PRI as

$$y_m(t) = x_m(t) + w_m(t), \quad (5)$$

where $x_m(t)$ and $w_m(t)$ are the fraction of $x(t)$ and $w(t)$ for $mT_p \leq t < (m+1)T_p$. We shall focus on this continuous-time baseband received signal model in the sequel.

2) *Radar post-processing:* The main task of the pulse-Doppler radar is to identify $3L$ parameters $\{\tau_\ell, \nu_\ell, H_\ell\}_{\ell=1}^L$ from the received signal $y(t)$ during CPI as in (2). To this end, the classical pulse-Doppler radar system performs two sequential post-processing: i) fast-time and ii) slow-time processing. Applying the post-processing, we can obtain a discrete-time equivalent signal model.

Fast-time processing: The fast-time processing allows obtaining the discrete-time samples of the returned signal using matched filtering and sampling. After the matched filtering and sampling at the Nyquist rate $T_s = 1/B_s$, the receiver obtains the discrete-time samples.

Let $\bar{Y}_{n,m}$, $\bar{X}_{n,m}$, and $\bar{W}_{n,m}$ be the discrete-time received, target, and noise signals for the n th range bin during the m th PRI. Using these notations, we can rewrite the continuous-time input-output relationship in (5) as

$$\bar{Y}_{n,m} = \bar{X}_{n,m} + \bar{W}_{n,m}, \quad (6)$$

where $\bar{W}_{n,m}$ follows the complex Gaussian with zero-mean and variance $B_s N_0$, i.e., $\bar{W}_{n,m} \sim \mathcal{CN}(0, B_s N_0)$ and $\bar{X}_{n,m}$ contains the target information for the relevant parameters $\{\tau_\ell, \nu_\ell, H_\ell\}_{\ell=1}^L$ as defined in (4). Suppose the ℓ th target exists in the n th range bin, i.e., $\lfloor \tau_\ell/T_s \rfloor = n$ for $n \in \{0, \dots, N-1\}$. In this case, the target signal is defined as $\bar{X}_{n,m} = \sqrt{\beta_\ell} H_\ell e^{-j2\pi m \nu_\ell T_p}$. Whereas, if a target is absent in the n th range bin, $\bar{X}_{n,m}$ is assumed to be null, i.e., $\bar{X}_{n,m} = 0$.

Using unit impulse function $\delta[n]$, we can define the discrete-time target signal $\bar{X}_{n,m}$ in compact form:

$$\bar{X}_{n,m} = \sum_{\ell=1}^L \sqrt{\beta_\ell} H_\ell \delta[n - U_\ell] e^{-j2\pi m \nu_\ell T_p}, \quad (7)$$

where $U_\ell = \lfloor \tau_\ell / T_s \rfloor \in \{0, \dots, N-1\}$ is discrete random variable indicating the range information for the ℓ th target.

Slow-time processing: In the pulse-Doppler radar system, the receiver also performs the matched filtering along the pulse dimension to increase the received power of the target signals. Recall that $0 \leq \nu_\ell T_p \leq 1$ and the Doppler resolution is $1/MT_p$. The limited Doppler resolution allows distinguishing target Doppler frequencies in the discrete set, i.e., $\nu_\ell T_p \in \{0, \frac{1}{M}, \dots, \frac{M-1}{M}\}$. With the discrete Doppler frequencies, the target signal in (7) boils down to

$$\bar{X}_{n,m} = \sum_{\ell=1}^L \sqrt{\beta_\ell} H_\ell \delta[n - U_\ell] e^{-j2\pi m \frac{V_\ell}{M}}, \quad (8)$$

where $V_\ell \in \{0, \dots, M-1\}$ represents the Doppler bin index of the ℓ th target. For given range bin index $n \in \{0, 1, \dots, N-1\}$, the receiver takes an M -point discrete Fourier transform (DFT) operation as

$$\begin{aligned} A_{n,k} &= \frac{1}{\sqrt{M}} \sum_{m=0}^{M-1} \bar{X}_{n,m} e^{-j\frac{2\pi k}{M}m} \\ &= \sum_{\ell=1}^L \sqrt{\frac{\beta_\ell}{M}} H_\ell \delta[n - U_\ell] \sum_{m=0}^{M-1} e^{-jm\left(\frac{2\pi V_\ell}{M} - \frac{2\pi k}{M}\right)}. \end{aligned} \quad (9)$$

Using the fact that $\sum_{m=0}^{M-1} e^{-jm\left(\frac{2\pi V_\ell}{M} - \frac{2\pi k}{M}\right)} = M\delta[k - V_\ell]$, we can represent the (n, k) entry of the target signal as

$$A_{n,k} = \sum_{\ell=1}^L \sqrt{M\beta_\ell} H_\ell \delta[n - U_\ell] \delta[k - V_\ell]. \quad (10)$$

3) *Discrete-time signal model:* Let snr_n be the signal-to-noise ratio (SNR) of the n th range bin. From the radar equation in (3) and the target signal model in (10), the SNR under the target's presence in the n th range bin is defined as

$$\text{snr}_n = \frac{M}{B_s N_o} \frac{P_t G_t \sigma_{\text{rcs}} A_{\text{eff}}}{(4\pi)^2 \bar{d}_n^4}, \quad (11)$$

where \bar{d}_n denotes the average distance from the n th range bin to the receiver, i.e., $\bar{d}_n = \frac{(2n+1)T_s c}{4}$. Denoting $Y_{n,k} = \frac{1}{\sqrt{M}} \sum_{m=0}^{M-1} \bar{Y}_{n,m} e^{j\frac{2\pi mk}{M}}$ and $Z_{n,k} = \frac{1}{\sqrt{M}} \sum_{m=0}^{M-1} \bar{W}_{n,m} e^{j\frac{2\pi mk}{M}}$, the discrete-time input-output signal relationship for the (n, k) range-Doppler bin is given by

$$Y_{n,k} = \sqrt{\text{snr}_n} X_{n,k} + Z_{n,k}, \quad (12)$$

where $Z_{n,k}$ is the normalized noise, which follows the complex Gaussian with zero-mean and unit variance, i.e., $Z_{n,k} \sim \mathcal{CN}(0, 1)$. From (10), we model that target returned signal $X_{n,k}$ is distributed as a Bernoulli-Gaussian (BG) random variable, i.e.,

$$f_{X_{n,k}}(x_{n,k}) = (1 - \gamma)\delta(x_{n,k}) + \gamma \frac{1}{\pi\sigma_T^2} e^{-\frac{(x_{n,k} - \mu_T)^2}{\sigma_T^2}}, \quad (13)$$

where $\gamma \in (0, 1)$ determines the probability that $X_{n,k}$ is a non-zero value. We shall use a short notation $X_{n,k} \sim \text{BG}(x|\mu_T, \sigma_T^2, \gamma)$ in the sequel.

Remark 1. The parameter γ determines the sparsity level of $X_{n,k}$ in the range-Doppler plane. This parameter γ contains a prior knowledge about environment. For instance, if the system is blind to the environment, one can choose $\gamma = 1/2$. However, when L targets on average have been detected in the previous CPIs, one can choose $\gamma = \frac{L}{MN}$. In this work, we focus on the specific CPI and assume γ to be a pre-determined parameter.

B. Performance Metrics

We shall characterize the *sensing spectral efficiency* of the pulse-Doppler radar system. An information theoretical approach to measure the information rate between $X_{n,k}$ and $Y_{n,k}$ is given by

$$R_{n,k}(\text{snr}_n) = I(X_{n,k}; Y_{n,k}) \quad (\text{bits/sec/Hz}), \quad (14)$$

for $n \in \{0, 1, \dots, N-1\}$ and $k \in \{0, 1, \dots, M-1\}$. It is noteworthy that the number of range bins N depends on the bandwidth ratio λ according to the Rayleigh criterion, which states that the range resolution is the inverse of the signal bandwidth [13]. This mutual information measures the amount of information acquired from the environment placed at the (n, k) range-Doppler bin. Since the mutual information differs across the range bins only, we define the average sensing rate as

$$R_s(B_s, \text{snr}_n) = \frac{B_s}{NM} \sum_{n=0}^{N-1} \sum_{k=0}^{M-1} R_{n,k}(\text{snr}_n) \quad (\text{bits/sec}). \quad (15)$$

This average information rate is the amount of information attained by sensing the target environment per second.

For the communication system, we consider the Gaussian channel. In the Gaussian channel, the communication rate with bandwidth B_c is given by

$$R_c(B_c, \text{snr}_c) = B_c \log_2(1 + \text{snr}_c) \quad (\text{bits/sec}), \quad (16)$$

where snr_c is the received SNR of communication system. Intuitively, increasing bandwidth for the range-Doppler radar system can improve sensing rate R_s while decreasing communication rate R_c . As a result, it is crucial to understand a trade-off between the sensing and communication rates according to the bandwidth ratio λ . To measure this trade-off, we define a weighted sum spectral efficiency as

$$R_{\text{sum}} = \frac{w_s R_s(B_s, \text{snr}_s) + w_c R_c(B_c, \text{snr}_c)}{B_s + B_c} \quad (\text{bits/sec/Hz}), \quad (17)$$

where w_s and w_c are weights for sensing and communication rates, respectively.

Remark 2. The system weights w_s and w_c can be chosen according to priority aspects of sensing and communication functions. For instance, the communication system for emergency broadcasting system is assigned higher than system for usual data transmission. The intrinsic disparity of two system can be incorporated into those weights [17]. The sensing system requires more power to obtain 1 bit than communication system because sensing system is regarded as uncooperative communication system. The high power demanding system weight can be assigned to be higher than other systems.

III. BAYESIAN TARGET ESTIMATION AND DETECTION

In this section, we first derive the MSE-optimal target estimation technique. Then, we show that both a maximum a posteriori (MAP) target detector, which minimizes the average target detection error, and Neyman-Pearson detector are special cases of the MSE-optimal target estimator.

A. MMSE Target Estimation

The main task of the range-Doppler radar is to identify the non-zero entries from the measurement matrix $\mathbf{Y} \in \mathbb{C}^{N \times K}$, which contains the target information during CPI. Since target signals $X_{n,k}$ and $X_{n',k'}$ are assumed to be statistically independent of $n \neq n'$ and $k \neq k'$, it is sufficient to design a target estimator for individual range-Doppler bin.

Recall the received signal of the (n, k) range-Doppler bin $Y_{n,k} = X_{n,k} + Z_{n,k}$ in (12). The mean and variance of $X_{n,k} \sim \text{BG}(x|\mu_{\text{T}}, \sigma_{\text{T}}^2, \gamma)$ are given by

$$\mathbb{E}[X_{n,k}] = \gamma\mu_{\text{T}} \quad \text{and} \quad \text{Var}[X_{n,k}] = \gamma(1 - \gamma)|\mu_{\text{T}}|^2 + \gamma\sigma_{\text{T}}^2. \quad (18)$$

Under the Gaussian measurement noise $Z_{n,k} \sim \mathcal{N}(0, 1)$, it is evident that the posterior distribution $P_{X_{n,k}|Y_{n,k}}(x_{n,k}|y_{n,k})$ also follows a BG distribution with different parameters $(\hat{\mu}_n, \hat{\sigma}_n^2, \hat{\gamma})$ because $Y_{n,k}$ is distributed as a BG random variable. The parameter $\hat{\mu}_n$ is the posterior mean conditioned that $X_{n,k} \neq 0$, which is computed as

$$\begin{aligned} \hat{\mu}_n &= \mathbb{E}[X_{n,k}|Y_{n,k} = y_{n,k}, X_{n,k} \neq 0; \text{snr}_n] \\ &= \mu_{\text{T}} + \frac{\sqrt{\text{snr}_n}\sigma_{\text{T}}}{1 + \text{snr}_n\sigma_{\text{T}}^2} (y_{n,k} - \sqrt{\text{snr}_n}\mu_{\text{T}}). \end{aligned} \quad (19)$$

The parameter $\hat{\sigma}_n^2$ is the posterior variance conditioned that $X_{n,k} \neq 0$. This conditional variance is equivalent to the well-known MMSE under the Gaussian prior, i.e.,

$$\begin{aligned} \hat{\sigma}_n^2 &= \text{Var}[X_{n,k}|Y_{n,k}, X_{n,k} \neq 0; \text{snr}_n] \\ &= \frac{\sigma_{\text{T}}^2}{1 + \text{snr}_n\sigma_{\text{T}}^2}. \end{aligned} \quad (20)$$

The last parameter $\hat{\gamma}_n$ is the posterior probability of a target existence, which is given by the following lemma.

Lemma 1. *Given $Y_{n,k} = y_{n,k}$, the posterior probability that a target signal is non-zero is given by*

$$\begin{aligned} \hat{\gamma}_n(y_{n,k}) &= \mathbb{P}[X_{n,k} \neq 0|Y_{n,k} = y_{n,k}] \\ &= \left[1 + \frac{1 - \gamma}{\gamma} (\text{snr}_n\sigma_{\text{T}}^2 + 1) e^{-|y_{n,k}|^2 + \frac{|y_{n,k} - \sqrt{\text{snr}_n}\mu_{\text{T}}|^2}{\text{snr}_n\sigma_{\text{T}}^2 + 1}} \right]^{-1}. \end{aligned} \quad (21)$$

Proof. See Appendix A. □

The following theorem presents the MSE-optimal target estimator and the corresponding MMSE.

Theorem 1. *The MMSE estimator for the target signal in the (n, k) range-Doppler bin is given by*

$$\begin{aligned}\hat{X}_{n,k}^{\text{mmse}}(y_{n,k}; \text{snr}_n) &= \mathbb{E}[X_{n,k} | Y_{n,k} = y_{n,k}; \text{snr}_n] \\ &= \frac{\mu_{\text{T}} + \frac{\sqrt{\text{snr}_n} \sigma_{\text{T}}}{1 + \text{snr}_n \sigma_{\text{T}}^2} (y_{n,k} - \sqrt{\text{snr}_n} \mu_{\text{T}})}{1 + \frac{1-\gamma}{\gamma} (\text{snr}_n \sigma_{\text{T}}^2 + 1) e^{-|y_{n,k}|^2 + \frac{|y_{n,k} - \sqrt{\text{snr}_n} \mu_{\text{T}}|^2}{\text{snr}_n \sigma_{\text{T}}^2 + 1}}}.\end{aligned}\quad (22)$$

The resultant MMSE is given by

$$\begin{aligned}\text{mmse}_{n,k}(\text{snr}_n) &= \mathbb{E} \left[\left(X_{n,k} - \hat{X}_{n,k}^{\text{mmse}}(Y_{n,k}) \right)^2; \text{snr}_n \right] \\ &= \int_{y \in \mathbb{C}} \left\{ \hat{\gamma}_n(y) (1 - \hat{\gamma}_n(y)) \left| \mu_{\text{T}} + \frac{\sqrt{\text{snr}_n} \sigma_{\text{T}}}{1 + \text{snr}_n \sigma_{\text{T}}^2} (y - \sqrt{\text{snr}_n} \mu_{\text{T}}) \right|^2 \right. \\ &\quad \left. + \hat{\gamma}_n(y) \left[\frac{\sigma_{\text{T}}^2}{1 + \text{snr}_n \sigma_{\text{T}}^2} \right]^2 \right\} f_{Y_{n,k}}(y) dy,\end{aligned}\quad (23)$$

where $f_{Y_{n,k}}(y)$ is a probability density function of a mixture-Gaussian random variable $Y_{n,k}$, i.e.,

$$f_{Y_{n,k}}(y) = (1 - \gamma) \frac{1}{\pi} e^{-|y|^2} + \gamma \frac{1}{\pi (\text{snr}_n \sigma_{\text{T}}^2 + 1)} e^{-\frac{|y - \sqrt{\text{snr}_n} \mu_{\text{T}}|^2}{\text{snr}_n \sigma_{\text{T}}^2 + 1}}. \quad (24)$$

Proof. The proof is direct by invoking (19), (20), and (21) into (18). \square

The derived MMSE estimator in Theorem 1 guarantees the optimal reconstruction quality in terms of MSE if the target signal distribution follows a BG distribution, $X_{n,k} \sim \text{BG}(x | \mu_{\text{T}}, \sigma_{\text{T}}^2, \gamma)$. The noticeable difference with the classical MMSE estimator for the Gaussian prior is a multiplicative parameter by $\hat{\gamma}_n$ defined in (21), which captures the chance to detect a target for given measurement $y_{m,k}$. The derived MMSE estimator can also be interpreted with a lens through a denoising function in imaging processing. The measurement data matrix $\mathbf{Y} \in \mathbb{C}^{N \times M}$ can be regarded as containing a two-dimensional complex target image $\mathbf{X} \in \mathbb{C}^{N \times M}$. The leading role of the MMSE estimator is to reduce noise signals; thereby, it constructs a more clear target image than \mathbf{Y} . This role differs from classical radar detectors, whose primary goal is to detect the target presence in a range-Doppler plane.

B. Connection to Classical Radar Detectors

To provide a more clear understanding of the derived MMSE radar detector, it is instructive to compare it with two classical radar detectors: i) MAP and ii) Neyman-Pearson (NP) detectors. Let us consider a binary target detector $g(\cdot) : \mathbb{C} \rightarrow \{0, 1\}$ which maps received signal $Y_{n,k}$ to a

binary value according to the target presence. Armed with this binary detector, we define two types of probability errors: i) false alarm probability P_{FA} and misdetection probability P_{MD} as

$$P_{\text{FA}}(\text{snr}_n) = \mathbb{P}[g(Y_{n,k}) = 1 \mid X_{n,k} = 0] \text{ and } P_{\text{MD}}(\text{snr}_n) = \mathbb{P}[g(Y_{n,k}) = 0 \mid X_{n,k} \neq 0]. \quad (25)$$

Then, an average probability error is given by

$$P_{\text{E}}(\gamma, \text{snr}_n) = \gamma P_{\text{MD}}(\text{snr}_n) + (1 - \gamma) P_{\text{FA}}(\text{snr}_n). \quad (26)$$

The MAP detector that minimizes the average probability error, $g_{\text{MAP}}(\cdot) = \arg \min_{g(\cdot)} P_{\text{E}}$, is given by

$$g_{\text{MAP}}(Y_{n,k}) = \begin{cases} 0, & \frac{\mathbb{P}(X_{n,k} \neq 0 \mid Y_{n,k})}{\mathbb{P}(X_{n,k} = 0 \mid Y_{n,k})} < 1, \\ 1, & \frac{\mathbb{P}(X_{n,k} \neq 0 \mid Y_{n,k})}{\mathbb{P}(X_{n,k} = 0 \mid Y_{n,k})} > 1. \end{cases} \quad (27)$$

From Lemma 1, the ratio of the posterior probabilities can be expressed as $\frac{\mathbb{P}(X_{n,k} \neq 0 \mid Y_{n,k} = y_{n,k})}{\mathbb{P}(X_{n,k} = 0 \mid Y_{n,k} = y_{n,k})} = \frac{\hat{\gamma}_n(y_{n,k})}{1 - \hat{\gamma}_n(y_{n,k})}$. Using this ratio, the MAP decision rule boils down to

$$g_{\text{MAP}}(Y_{n,k}) = \begin{cases} 0, & \frac{\hat{\gamma}_n(Y_{n,k})}{1 - \hat{\gamma}_n(Y_{n,k})} < 1, \\ 1, & \frac{\hat{\gamma}_n(Y_{n,k})}{1 - \hat{\gamma}_n(Y_{n,k})} > 1. \end{cases} \quad (28)$$

When establishing the MAP detector, the posterior probability of the target presence $\hat{\gamma}_n(y_{n,k})$ in (21) is sufficient information. The MMSE estimator, however, requires additional information about $\hat{\mu}_n$ in (19) and $\hat{\sigma}_n^2$ in (20) beyond $\hat{\gamma}_n(y_{n,k})$. This fact reveals that the classical MAP detector is a special case of the MMSE estimator when discarding information about $\hat{\mu}_n$ and $\hat{\sigma}_n^2$.

Unlike the Bayesian approach using a prior distribution, a classical detector in radar theory does not exploit prior information of the target signal because of the absence of such knowledge in general. According to the celebrated NP rule, the optimal binary detector $g_{\text{NP}}(Y_{n,k})$ with threshold δ can be defined with the likelihood ratios as

$$g_{\text{NP}}(Y_{n,k}) = \begin{cases} 0, & \frac{\mathbb{P}(Y_{n,k} \mid X_{n,k} \neq 0)}{\mathbb{P}(Y_{n,k} \mid X_{n,k} = 0)} < \delta, \\ 1, & \frac{\mathbb{P}(Y_{n,k} \mid X_{n,k} \neq 0)}{\mathbb{P}(Y_{n,k} \mid X_{n,k} = 0)} > \delta. \end{cases} \quad (29)$$

The threshold parameter δ can be chosen to minimize P_{FA} subject to a constraint of $P_{\text{MD}} = \alpha$ with $\alpha > 0$, which is referred to as NP detector. This NP detector can be deduced from the posterior probability of the target presence $\hat{\gamma}_n(y_{n,k})$ in (21). By applying Bayes' rule to likelihood ratio

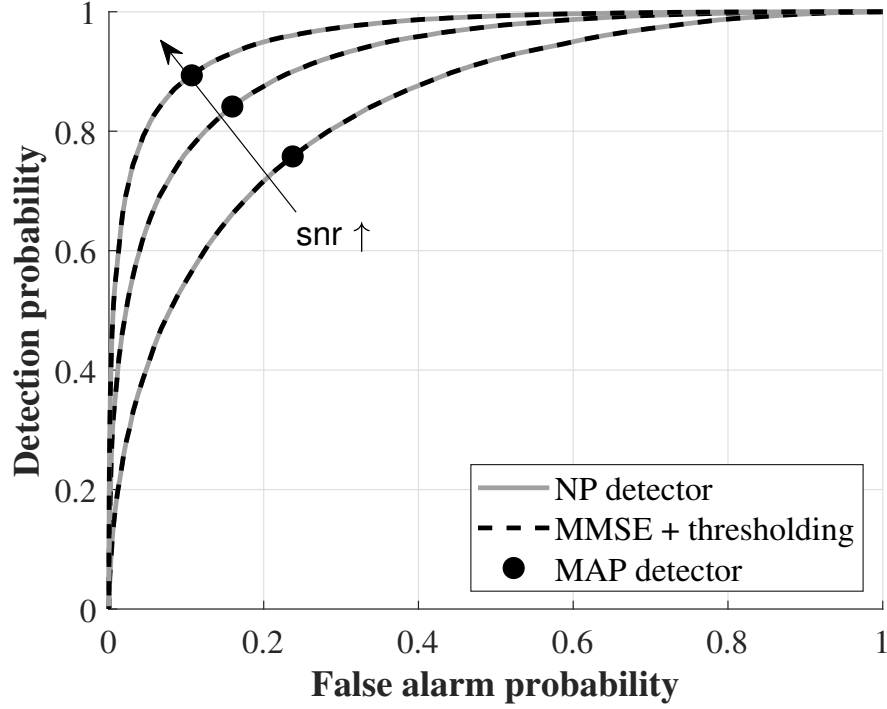


Fig. 2. ROC curves for three different types of detectors: i) NP, ii) MMSE estimator with hard threshold, and iii) MAP detectors. Target parameters are set to be $\gamma = 0.5$, $\mu_T = 1$, $\sigma_T^2 = 10^{-1}$, $\text{snr}_n \in \{0, 3, 5\}$ [dB].

to obtain the identity $\frac{\mathbb{P}(Y_{n,k}|X_{n,k} \neq 0)}{\mathbb{P}(Y_{n,k}|X_{n,k} = 0)} = \frac{\mathbb{P}(X_{n,k} \neq 0|Y_{n,k}) \mathbb{P}(X_{n,k} = 0)}{\mathbb{P}(X_{n,k} = 0|Y_{n,k}) \mathbb{P}(X_{n,k} \neq 0)} = \frac{\hat{\gamma}_n(Y_{n,k})}{1 - \hat{\gamma}_n(Y_{n,k})} \frac{1 - \gamma}{\gamma}$, the NP criterion reduces to

$$g_{\text{NP}}(Y_{n,k}) = \begin{cases} 0, & \frac{\hat{\gamma}_n(Y_{n,k})}{1 - \hat{\gamma}_n(Y_{n,k})} < \frac{\gamma}{1 - \gamma} \delta, \\ 1, & \frac{\hat{\gamma}_n(Y_{n,k})}{1 - \hat{\gamma}_n(Y_{n,k})} > \frac{\gamma}{1 - \gamma} \delta. \end{cases} \quad (30)$$

In addition, it is worthwhile mentioning that the MAP detector in (28) is equivalent to the NP detector if the threshold parameter is chosen as $\delta = (1 - \gamma)/\gamma$.

To find the error probability expressions, we define the region as

$$\mathcal{A}(\text{snr}_n) = \{y_{n,k} \in \mathbb{C} \mid \hat{\gamma}_n(y_{n,k})(1 - \gamma) > (1 - \hat{\gamma}_n(y_{n,k})) \gamma \delta\}. \quad (31)$$

Then, the false alarm probability P_{FA} and misdetection probability P_{MD} when using the NP detector are given by

$$P_{\text{FA}}(\text{snr}_n) = \int_{y \in \mathcal{A}(\text{snr}_n)} \frac{1}{\pi} e^{-|y|^2} dy, \quad (32)$$

$$P_{\text{MD}}(\text{snr}_n) = \int_{y \notin \mathcal{A}(\text{snr}_n)} \frac{1}{\pi (\text{snr}_n \sigma_T^2 + 1)} e^{-\frac{|y - \sqrt{\text{snr}_n} \mu_T|^2}{\text{snr}_n \sigma_T^2 + 1}} dy. \quad (33)$$

To clearly show the generality of the MMSE estimator, we compare the proposed MMSE estimator with the classical NP detector and MAP detector using a receiver operating characteristic (ROC) curve. As shown in Fig. 2, our MMSE detector with a proper choice threshold can achieve identical ROC curves with the NP detector. This result shows that the MMSE detector is deeply connected to the classical NP detector. At the same time, it helps to define the sensing rate from an information-theoretical viewpoint.

IV. SENSING RATE CHARACTERIZATION

In this section, we express the sensing rate in terms of estimation-theoretic quantity by applying the I-MMSE relationship in [29]. To provide a better understanding of the sensing rate in terms of target parameters, we present a lower bound of the sensing rate by decomposing it into two parts. Furthermore, we derive approximation of sensing rates with a closed-form. These tractable expressions will be stepping stones toward finding the optimal bandwidth strategy for ISAC systems in the sequel.

A. An Exact Expression

The I-MMSE relationship is a foundation that provides a deep connection between an information- and an estimation-theoretic quantity [29]. The I-MMSE relationship states that the integration of MMSE is the mutual information for an arbitrary target distribution $f_{X_{n,k}}(x_{n,k})$ with a finite moment $\mathbb{E}[X_{n,k}^2] < \infty$ [29]. From this statement and the derived MMSE in (23), we can formally define the sensing rate of a pulse-Doppler radar system.

Theorem 2. *The sensing rate $R_{n,k}(\text{snr}_n) = I(X_{n,k}; Y_{n,k})$ for (n, k) range-Doppler bin is given by*

$$R_{n,k}(\text{snr}_n) = \log_2 e \int_0^{\text{snr}_n} \text{mmse}_{n,k}(s) ds. \quad (34)$$

Proof. The proof is the direct consequence from MMSE in Theorem 1 and the I-MMSE relationship in [29]. \square

From Theorem 2, it is evident that the information rate is an increasing function with snr_n by the non-negativity of $\text{mmse}_{n,k}(s)$ for $s > 0$. Although the expression in (34) is exact and has full generality, this analytical expression of the sensing rate is intractable to understanding how the target parameters, $(\mu_T, \sigma_T, \gamma)$, change the information rate.

B. A Lower Bound

To shed light on the insight in Theorem 2, we provide a lower bound of the sensing rate in the following Theorem.

Theorem 3. *Let $H_b(p) = -p \log p - (1-p) \log(1-p)$ be a binary entropy function with parameter $p \in [0, 1]$. Then, the sensing rate for the (n, k) range-Doppler bin $I(X_{n,k}; Y_{n,k})$ is lower bounded by*

$$I(X_{n,k}; Y_{n,k}) \geq H_b(\gamma) - H_{\text{NP}}(\gamma, P_{\text{FA}}, P_{\text{MD}}) + \gamma \log_2(1 + \text{snr}_n \sigma_{\text{T}}^2), \quad (35)$$

where P_{FA} and P_{MD} is the false alarm and misdetection error probability of (30) and

$$H_{\text{NP}}(\gamma, P_{\text{FA}}, P_{\text{MD}}) = H_b(\gamma) + (1 - \gamma)H_b(P_{\text{FA}}) + \gamma H_b(P_{\text{MD}}) - H_b((1 - \gamma)P_{\text{FA}} + \gamma(1 - P_{\text{MD}})). \quad (36)$$

Proof. We first define a binary random variable $U_{n,k} \in \{0, 1\}$ with Bernoulli parameter γ to denote the target presence at the (n, k) range-Doppler bin. Similarly, we introduce the target complex amplitude parameter $A_{n,k}$, which is drawn from $\mathcal{CN}(\mu_{\text{T}}, \sigma_{\text{T}}^2)$. Then, our BG target signal $X_{n,k} \sim \text{BG}(x|\mu_{\text{T}}, \sigma_{\text{T}}^2, \gamma)$ can be represented in a vector form $(U_{n,k}, A_{n,k})$. Using the chain rule, we decompose the mutual information as

$$\begin{aligned} I(X_{n,k}; Y_{n,k}) &= I(U_{n,k}, A_{n,k}; Y_{n,k}) \\ &= I(U_{n,k}; Y_{n,k}) + I(A_{n,k}; Y_{n,k} | U_{n,k}) \\ &= I(U_{n,k}; Y_{n,k}) + (1 - \gamma)I(A_{n,k}; Y_{n,k} | U_{n,k} = 0) + \gamma I(A_{n,k}; Y_{n,k} | U_{n,k} = 1) \\ &= I(U_{n,k}; Y_{n,k}) + \gamma \log_2(1 + \text{snr}_n \sigma_{\text{T}}^2), \end{aligned} \quad (37)$$

where the last equality comes from $I(A_{n,k}; Y_{n,k} | U_{n,k} = 0) = 0$.

We consider the NP detector to obtain the lower bound of $I(U_{n,k}; Y_{n,k})$. Let $\hat{Y}_{n,k}$ be the output of the NP detector. Then, we can form the Markov chain $U_{n,k} \rightarrow Y_{n,k} \rightarrow \hat{Y}_{n,k}$. From the processing inequality, we have $I(U_{n,k}; Y_{n,k}) \geq I(U_{n,k}; \hat{Y}_{n,k})$. By noticing that $U_{n,k}$ and $\hat{Y}_{n,k}$ are the input and output of a binary asymmetric channel, we can lower bound the target detection information as

$$\begin{aligned} I(U_{n,k}; Y_{n,k}) &\geq I(U_{n,k}; \hat{Y}_{n,k}) \\ &= H_b((1 - \gamma)P_{\text{FA}} + \gamma(1 - P_{\text{MD}})) - (1 - \gamma)H_b(P_{\text{FA}}) - \gamma H_b(P_{\text{MD}}). \end{aligned} \quad (38)$$

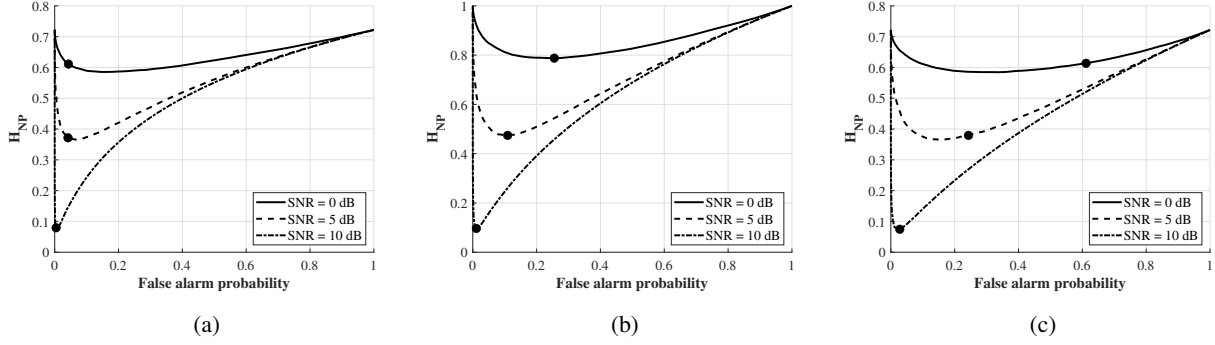


Fig. 3. Remaining uncertainty $H_{NP}(\gamma, P_{FA}, P_{MD})$ after detection and false alarm probability P_{FA} when applying NP detector. The circle marker is obtained by MAP detector. Target statistics: $\mu_T = 1$, $\sigma_T^2 = 0$, $\text{snr}_n \in \{0, 5, 10\}$ [dB]. (a) $\gamma = 0.2$, (b) $\gamma = 0.5$, (c) $\gamma = 0.8$.

Plugging (38) into (37), we obtained the expression, which completes the proof. \square

Theorem 3 elucidates how the sensing rate changes according to the target parameters and target detector. To be specific, the sensing rate can be decomposed into three parts. The first part $H_b(\gamma)$ measures the uncertainty of the target localized at a specific (n, k) range-Doppler bin. In other words, this part provides the target's location and velocity information in a two-dimensional data matrix. This information rate increases with the underlying target presence probability γ in the system, which aligns with our intuition that more target presence likelihood increases the sensing rate. This information rate, however, is reduced by the target detection error, $H_{NP}(\gamma, P_{FA}, P_{MD})$. As a result, the sensing rate can diminish as the error probability increases (e.g., low SNR or using sub-optimal detectors) as shown in Fig. 3. The last part $\gamma \log_2(1 + \text{snr}_n \sigma_T^2)$ measures the amount of information rate acquired from the target's returned signal under the target presence with probability γ . This rate is proportional to both the target's presence probability γ and the target signal variance σ_T^2 for given SNR.

C. Approximation of Sensing Rate

Although the lower bound in Theorem 3 is useful in understanding the sensing rate in terms of the relevant system parameters, it is still unwieldy to compute the sensing rate because the detection error probability computation involves some numerical integrals. To remedy this issue,

we provide a tight approximate expression of the sensing rate in closed-form, which is stated in the following theorem.

Theorem 4. *The sensing rate for the (n, k) range-Doppler bin $R_{n,k}(\text{snr}_n) = I(X_{n,k}; Y_{n,k})$ is tightly approximated as*

$$R_{n,k}(\text{snr}_n) \approx H_b(\gamma) - \hat{H}(T|Y) + \gamma \log_2 (1 + \text{snr}_n \sigma_T^2), \quad (39)$$

where the approximated conditional entropy $\hat{H}(T|Y)$ is given by

$$\begin{aligned} \hat{H}(T|Y) = & (1 - \gamma) \log_2 \left(1 + \frac{\gamma}{1 - \gamma} \frac{2}{2 + \text{snr}_n \sigma_T^2} e^{-\frac{\text{snr}_n |\mu_T|^2}{2 + \text{snr}_n \sigma_T^2}} \right) \\ & + \gamma \log_2 \left(1 + \frac{1 - \gamma}{\gamma} \frac{2(1 + \text{snr}_n \sigma_T^2)}{2 + \text{snr}_n \sigma_T^2} e^{-\frac{\text{snr}_n |\mu_T|^2}{2 + \text{snr}_n \sigma_T^2}} \right). \end{aligned} \quad (40)$$

Proof. See Appendix B. □

As shown in Theorem 4, the approximate rate expression can be composed into three parts as derived in Theorem 3. The difference is the second part, conditional entropy. Although this expression is an approximation of the conditional entropy, it still has full generality to capture the effect of target parameters $(\gamma, \mu_T, \sigma_T^2)$. In addition, the closed-form expression drastically reduces the computation time required for the evaluation of the sensing rate by facilitating the bandwidth allocation problem for the ISAC system in the next section.

V. OPTIMAL BANDWIDTH ALLOCATION FOR ISAC

In this section, we consider the bandwidth allocation problem for the ISAC system. Recall that the weighted sum spectral efficiency in (17) involves the trade-off in terms of the bandwidth ratio λ because the radar bandwidth B_s and the communication bandwidth B_c is a function of ratio λ . In particular, the signal-to-noise ratio of each system (i.e., snr_n and snr_c) relies on the allocated bandwidth B_s and B_c , or ratio λ . In addition, the number of range bins N is given by the inverse of the radar bandwidth B_s . For simplicity, we assume that the target parameters

$(\gamma, \mu_T, \sigma_T^2)$ and transmit power P_t are constants when allocating the bandwidth, and introduce the following notations to express the dependency on λ explicitly:

$$\text{snr}_c(\lambda) = \frac{\rho_c}{1-\lambda} = \frac{P_t}{(1-\lambda)BN_0}, \quad (41)$$

$$\text{snr}_n(\lambda) = \frac{\rho_n}{\lambda} = \frac{M}{\lambda BN_o} \frac{P_t G_t \sigma_{\text{rcs}} A_{\text{eff}}}{(4\pi)^2 \bar{d}_n^4}, \quad (42)$$

$$R_c(\lambda) = (1-\lambda)B \log_2 \left(1 + \frac{\rho_c}{1-\lambda} \right), \quad (43)$$

$$R_s(\lambda) = \frac{\lambda B}{N(\lambda)K} \sum_{n=0}^{N(\lambda)-1} \sum_{k=0}^{M-1} R_{n,k}(\text{snr}_n(\lambda)), \quad (44)$$

$$R_{\text{sum}}(\lambda) = \frac{w_s R_s(\lambda) + w_c R_c(\lambda)}{B}. \quad (45)$$

We aim to allocate the bandwidth to maximize the weighted sum spectral efficiency in (45) by solving the following optimization problem:

$$\lambda^* = \underset{0 \leq \lambda \leq 1}{\text{argmax}} R_{\text{sum}}(\lambda). \quad (46)$$

Unfortunately, the objective function $R_{\text{sum}}(\lambda)$ is not differentiable for λ because the number of addition in $R_s(\lambda)$ depends on λ , which hinders the development of efficient optimization algorithm. To circumvent this difficulty and to get an insight into the bandwidth allocation result, we assume that all the range-Doppler bins have the same $\text{snr}_s(\lambda)$. By choosing $\overline{\text{snr}}_s(\lambda) = \text{snr}_{N-1}(\lambda)$ (i.e., the smallest SNR), we can lower bound the sensing rate in the objective function as

$$\begin{aligned} R_s(\lambda) &= \frac{\lambda B}{N(\lambda)M} \sum_{n=0}^{N(\lambda)-1} \sum_{k=0}^{M-1} R_{n,k}(\text{snr}_n(\lambda)) \\ &\geq \frac{\lambda B}{N(\lambda)M} \sum_{n=0}^{N(\lambda)-1} \sum_{k=0}^{M-1} R_{n,k}(\text{snr}_{N-1}(\lambda)) \\ &= \lambda B R_{n,k}(\overline{\text{snr}}_s(\lambda)) \\ &\triangleq \bar{R}_s(\lambda) \end{aligned} \quad (47)$$

If we define $\bar{R}_{\text{sum}}(\lambda) = w_s \bar{R}_s(\lambda) + w_c R_c(\lambda)$, then we have the following bandwidth allocation problem for the ISAC system:

$$\bar{\lambda}^* = \underset{0 \leq \lambda \leq 1}{\text{argmax}} \bar{R}_{\text{sum}}(\lambda). \quad (48)$$

Now, we present the Karush-Kuhn-Tucker (KKT) optimality conditions for the optimization problem in (48).

Theorem 5. *The KKT condition of (48) is satisfied if we choose $\bar{\lambda}^* \in [0, 1]$ such that*

$$w_s \left. \frac{d\bar{R}_s(\lambda)}{d\lambda} \right|_{\lambda=\bar{\lambda}^*} + w_c \left. \frac{dR_c(\lambda)}{d\lambda} \right|_{\lambda=\bar{\lambda}^*} = 0. \quad (49)$$

If there is no such $\bar{\lambda}^ \in [0, 1]$, then it is given by*

$$\bar{\lambda}^* = \begin{cases} 1, & w_s \frac{d\bar{R}_s(\lambda)}{d\lambda} > -w_c \frac{dR_c(\lambda)}{d\lambda}, \\ 0, & w_s \frac{d\bar{R}_s(\lambda)}{d\lambda} < -w_c \frac{dR_c(\lambda)}{d\lambda}. \end{cases} \quad (50)$$

In addition, $\bar{R}_s(\lambda)$ is increasing concave function with respect to λ and $R_c(\lambda)$ is monotonic decreasing concave function with respect to λ .

Proof. See Appendix C □

According to Theorem 5, the optimal bandwidth allocation ratio is determined by comparing the derivative of the rates with respect to λ . For a given ratio λ , the radar uses more bandwidth $d\lambda$ if the increased information of the radar system is larger than the decreased information of the communication system when we set the ratio to be $\lambda + d\lambda$. To provide a better understanding of Theorem 5, we offer the estimation theoretic interpretation of the change of the radar information when we allocate infinitesimal additional bandwidth to the radar system. By the I-MMSE relationship, we can express the derivative of the sensing rate as

$$\frac{dR_{n,k}(\overline{\text{snr}}_s(\lambda))}{d \overline{\text{snr}}_s(\lambda)} = \text{mmse}_{n,k}(\overline{\text{snr}}_s(\lambda)) \log_2 e. \quad (51)$$

Using this, we can rewrite the KKT condition as

$$w_s (R_{n,k}(\overline{\text{snr}}_s(\lambda)) - \overline{\text{snr}}_s(\lambda) \cdot \text{mmse}_{n,k}(\overline{\text{snr}}_s(\lambda)) \log_2 e) = -\frac{w_c}{B} \frac{dR_c(\lambda)}{d\lambda}. \quad (52)$$

As a result, the estimation quality of the radar system measured in terms of MMSE is compared with the reduction of the communication information rate when we determine the optimal bandwidth that maximizes the weighted sum information rates. In conclusion, it is more efficient for a radar system to use more bandwidth than the communication system in the following two cases: i) the radar estimation error (i.e., MMSE) compared to $\overline{\text{snr}}_s(\lambda)$ is small enough to compensate the decline of the information rate of the communication system, or ii) the information rate of the radar system is large enough to tolerate a significant estimation error. Finally, we put some remarks about Theorem 5.

Remark 3 (Bisection method for optimal bandwidth allocation). Because the left side of (49) is decreasing with respect to λ , the optimal bandwidth allocation ratio λ^* can be found by bisection method.

Remark 4 (Approximation strategy). To evaluate the KKT condition in (49), we need to compute complicated integral in (23) and (34), which is time-consuming. Instead, we can use the approximation expression in Theorem 4 to compute $\bar{R}_s(\lambda)$.

VI. NUMERICAL RESULTS

This section presents the numerical simulation results of the sensing rate and ISAC bandwidth allocation problem.

A. Sensing Rate

In this subsection, we verify the Theorem 3 and 4, each of which characterizes the lower bound and approximation of the sensing rate. In addition, we present the operational meaning of the sensing rate by using the decomposed expression to obtain a more detailed understanding.

Tightness of the lower bound and approximation: We provide numerical results to verify the exactness of the derived rate expression in Theorem 3 and Theorem 4. Fig. 4 shows that our lower bound and approximation expressions are very tight at all SNRs. This result confirms that our closed-form expression for the sensing rate is exact. In addition, we can use the approximation expression to find the optimal bandwidth allocation strategy for the ISAC system.

The decomposed information: To shed light on the behavior of sensing rate, we provide numerical results of *target detection information* and *target fluctuation information* separately in Fig. 5. Recall that the target detection mutual information is $I(U_{n,k}; Y_{n,k})$ and the target fluctuation mutual information is $I(A_{n,k}; Y_{n,k} | U_{n,k} = 1)$.

Fig. 5-(a) presents the decomposed information corresponding to various γ . We observe that the target detection information is dominant in the low SNR regime, and the target fluctuation information is dominant in the high SNR regime. It means that the target detection ability is important at low SNR. At a high SNR regime, the target signal estimation precision contributes to the sensing rate rather than target detection accuracy. Fig. 5-(b) is decomposed information displayed by switching σ_T^2 . The target detection information decreases as the target fluctuation σ_T^2 increases because the fluctuation hinders the target detection. Especially for MAP detector in

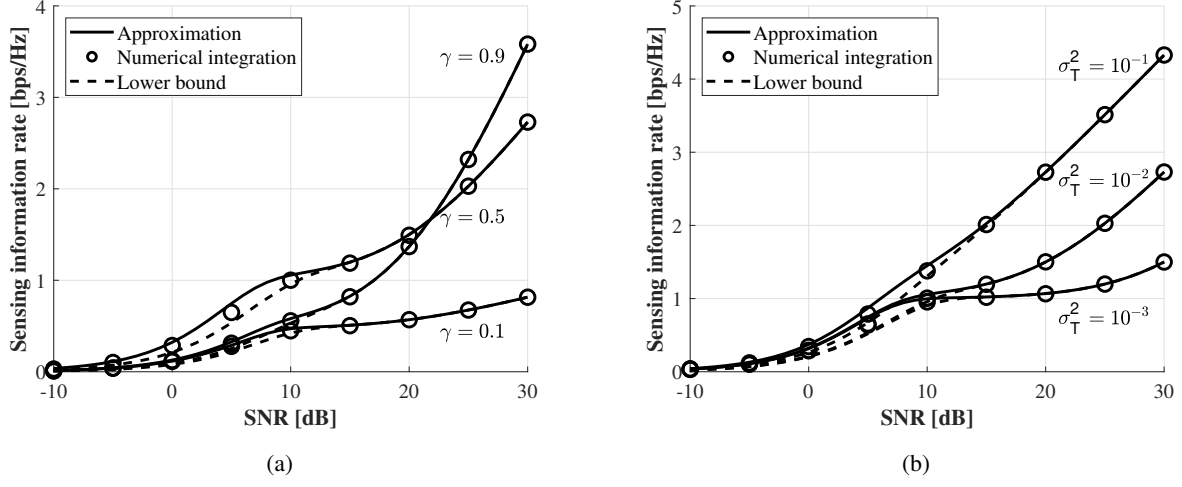


Fig. 4. Illustration to verify the tightness of the lower bound and approximation in Theorem 3 and 4. Target signal statistics: (a) $\gamma \in \{0.1, 0.5, 0.9\}$, $\mu_T = 1$, and $\sigma_T^2 = 10^{-2}$, (b) $\gamma = 0.5$, $\mu_T = 1$, and $\sigma_T^2 \in \{10^{-1}, 10^{-2}, 10^{-3}\}$.

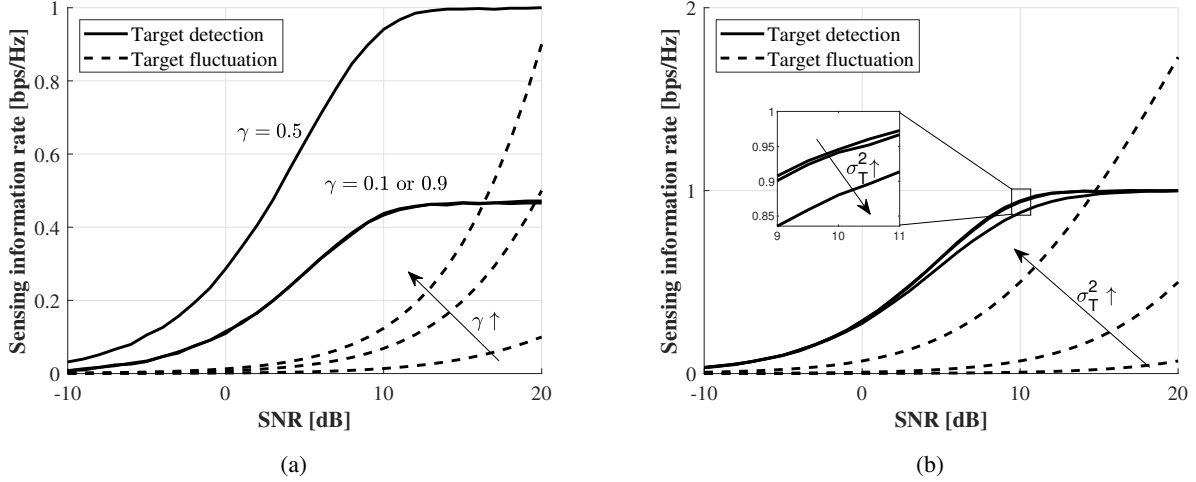


Fig. 5. Illustration of decomposed sensing rate. Target signal statistics: (a) $\gamma \in \{0.1, 0.5, 0.9\}$, $\mu_T = 1$, and $\sigma_T^2 = 10^{-2}$, (b) $\gamma = 0.5$, $\mu_T = 1$, and $\sigma_T^2 \in \{10^{-1}, 10^{-2}, 10^{-3}\}$.

(28), this fluctuation acts as additive noise; thereby, the probability of detection error increases. Since the probability of detection error is related to conditional entropy $H(U_{n,k}|Y_{n,k})$, the increased detection error yields the increased conditional entropy, and finally renders the decreased target detection information rate. As the target variance increases, the system can obtain more fluctuation information, and it originates from the increased target signal uncertainty.

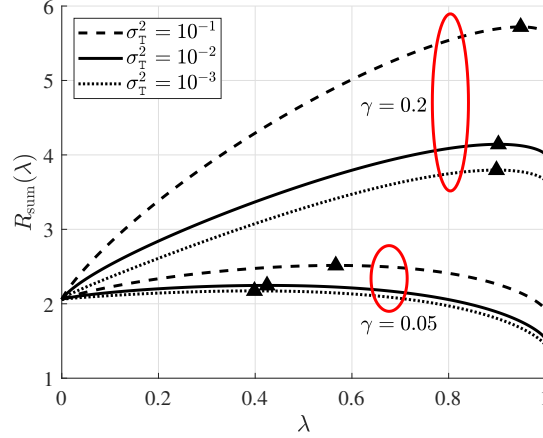


Fig. 6. Bandwidth allocation results depending on target statistics. The system weights are $w_s = 5$ and $w_c = 1$.

B. ISAC Bandwidth Allocation

Simulation setup: We assume that a total bandwidth is set to $B = 200$ MHz. We set $\text{snr}_c(0) = P_t/(BN_0) = 5$ dB for the communication system. For the radar system, we set $\overline{\text{snr}}_s(1) = \text{snr}_{N-1}(1) = 15$ dB and the maximum detection range as 10 km.

The effect of target statistics: We present the optimal bandwidth ratio λ^* and target statistics (γ, σ_T^2) in Fig. 6. The upper triangular marker indicates the optimal point. We find that both the amount of weighted sum spectral efficiency $\bar{R}_{\text{sum}}(\lambda)$ and the radar-allocated bandwidth increases as both of the target uncertainties γ and σ_T^2 increase. It is also noticeable that the amount of information increment caused by increased σ_T^2 becomes large when γ increases due to the larger target estimation information.

ISAC system trade-off: Fig. 7 presents the information rate trade-off of the ISAC system for various target statistics γ and σ_T^2 . The sensing rate increases gradually when the communication rate decreases. The behavior of the trade-off curve results from how γ is modeled depending on the sensing bandwidth and target statistics. In particular, we fix γ for each bin. Increasing the sensing bandwidth improves the resolution of the range-Doppler map. The increased resolution gives more chances to discover new targets in the environment.

VII. CONCLUSION

By utilizing an information-theoretic approach, we evaluated the performance of the ISAC system by characterizing the amount of information that the pulse-Doppler radar can obtain. First,

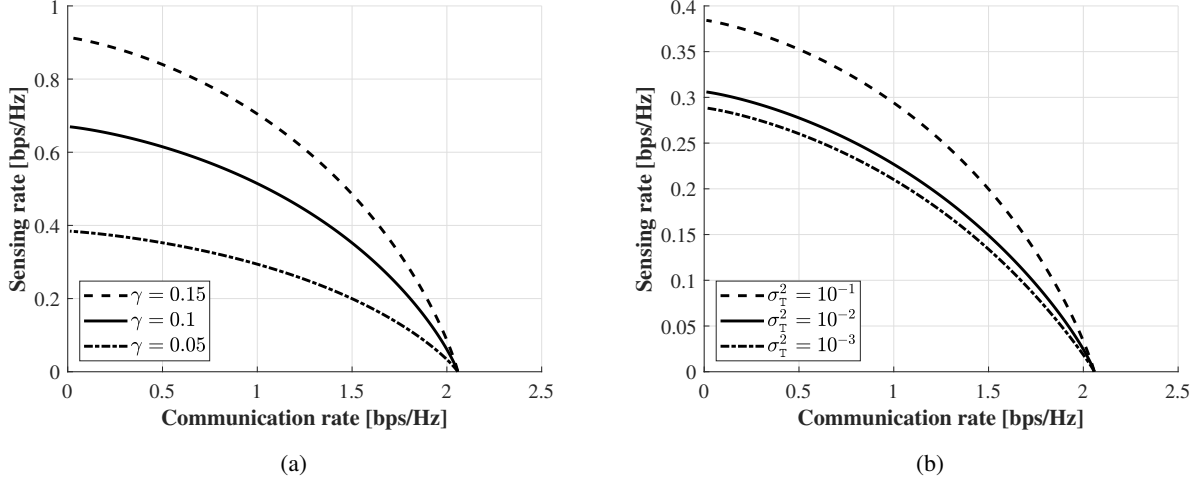


Fig. 7. Information rate of ISAC system according to target statistics γ and σ_T^2 . (a) $\gamma = 0.05$, (b) $\sigma_T^2 = 10^{-1}$.

we calculated the sensing rate of an unknown environment using the pulse-Doppler radar and established correlations with various radar system parameters. Then, by integrating the sensing rate, closed-form expressions, and Shannon's communication rate into the ISAC system, we derived an optimal bandwidth allocation strategy that maximizes the weighted sum spectral efficiency. Our findings indicated that when target uncertainty and SNR are high, more bandwidth should be allocated for the radar system. Our simulation results confirmed the accuracy of the derived closed-form expressions.

APPENDIX

A. Proof of Lemma 1

From Baye's rule, we compute

$$\begin{aligned} \mathbb{P}[X_{n,k} \neq 0 | Y_{n,k} = y_{n,k}] &= \frac{\mathbb{P}[X_{n,k} \neq 0 | Y_{n,k} = y_{n,k}] \mathbb{P}(Y_{n,k} = y_{n,k})}{\mathbb{P}(Y_{n,k} = y_{n,k})} \\ &= \frac{\mathbb{P}(X_{n,k} \neq 0, Y_{n,k} = y_{n,k})}{\mathbb{P}(X_{n,k} = 0, Y_{n,k} = y_{n,k}) + \mathbb{P}(X_{n,k} \neq 0, Y_{n,k} = y_{n,k})}. \end{aligned} \quad (53)$$

The joint probabilities are computed as

$$\begin{aligned} \mathbb{P}(X_{n,k} = 0, Y_{n,k} = y_{n,k}) &= \mathbb{P}(X_{n,k} = 0) \mathbb{P}(Y_{n,k} = y_{n,k} | X_{n,k} = 0) \\ &= (1 - \gamma) \frac{1}{\pi} e^{-|y_{n,k}|^2} \end{aligned} \quad (54)$$

and

$$\begin{aligned}\mathbb{P}(X_{n,k} \neq 0, Y_{n,k} = y_{n,k}) &= \mathbb{P}(X_{n,k} \neq 0) \mathbb{P}(Y_{n,k} = y_{n,k} | X_{n,k} \neq 0) \\ &= \gamma \times \frac{1}{\pi(\text{snr}_n \sigma_{\text{T}}^2 + 1)} e^{-\frac{|y_{n,k} - \sqrt{\text{snr}_n} \mu_{\text{T}}|^2}{\text{snr}_n \sigma_{\text{T}}^2 + 1}}.\end{aligned}\quad (55)$$

Invoking (54) and (55) into (53), we obtain the probability that the target is absent in the (n, k) range-Doppler bin as

$$\begin{aligned}\mathbb{P}[X_{n,k} \neq 0 | Y_{n,k} = y_{n,k}] &= \frac{\gamma \frac{1}{\pi(\text{snr}_n \sigma_{\text{T}}^2 + 1)} e^{-\frac{|y_{n,k} - \sqrt{\text{snr}_n} \mu_{\text{T}}|^2}{\text{snr}_n \sigma_{\text{T}}^2 + 1}}}{(1 - \gamma) \frac{1}{\pi} e^{-|y_{n,k}|^2} + \gamma \frac{1}{\pi(\text{snr}_n \sigma_{\text{T}}^2 + 1)} e^{-\frac{|y_{n,k} - \sqrt{\text{snr}_n} \mu_{\text{T}}|^2}{\text{snr}_n \sigma_{\text{T}}^2 + 1}}} \\ &= \frac{1}{1 + \frac{1-\gamma}{\gamma} (\text{snr}_n \sigma_{\text{T}}^2 + 1) e^{-|y_{n,k}|^2 + \frac{|y_{n,k} - \sqrt{\text{snr}_n} \mu_{\text{T}}|^2}{\text{snr}_n \sigma_{\text{T}}^2 + 1}}}.\end{aligned}\quad (56)$$

This completes the proof of lemma.

B. Proof of Theorem 4

The proof proceeds two-steps: i) finding a lower bound of entropy of $Y_{n,k}$ and ii) compensating an offset that occurred in an asymptotic regime, i.e., $\text{snr}_n \rightarrow 0$ and $\text{snr}_n \rightarrow \infty$. In this proof, we shall use the equivalent channel:

$$Y_{n,k} = X_{n,k} + Z_{n,k}, \quad Z_{n,k} \sim \mathcal{CN}\left(0, \frac{1}{\text{snr}_n}\right). \quad (57)$$

In addition, we drop the indices (n, k) for notational convenience.

First, the distribution of Y is given by

$$\begin{aligned}p(y) &= (1 - \gamma) \frac{\text{snr}}{\pi} \exp(-\rho |y|^2) + \gamma \frac{1}{\pi(\sigma_{\text{T}}^2 + \frac{1}{\text{snr}})} \exp\left(-\frac{|y - \mu_{\text{T}}|^2}{\sigma_{\text{T}}^2 + \frac{1}{\text{snr}}}\right) \\ &\triangleq \sum_{i=0}^1 w_i p_i(y),\end{aligned}\quad (58)$$

where $w_0 = 1 - \gamma$, $w_1 = \gamma$, $p_0(y) \sim \mathcal{CN}(0, 1/\text{snr})$, and $p_1(y) \sim \mathcal{CN}(\mu_{\text{T}}, \sigma_{\text{T}}^2 + (1/\text{snr}))$.

From [30], a lower bound of $H(Y)$ is computed as

$$\begin{aligned}
H(Y) &= - \sum_i w_i \int p_i(y) \log \sum_j w_j p_j(y) dy \\
&\geq - \sum_i w_i \log \int p_i(y) \sum_j w_j p_j(y) dy \\
&= - \sum_i w_i \log \sum_j w_j \underbrace{\left(\int p_i(y) p_j(y) dy \right)}_{\epsilon_{i,j}} \\
&\triangleq H_{\text{Low}}(Y).
\end{aligned} \tag{59}$$

For the complex Gaussian distribution $p_i(y)$ and $p_j(y)$, the integral $\epsilon_{i,j}$ in (59) can be further evaluated as follows:

$$\begin{aligned}
\epsilon_{i,j} &= \frac{1}{\pi^2 \sigma_i^2 \sigma_j^2} \int_{y \in \mathbb{C}} \exp \left(-\frac{|y - \mu_i|^2}{\sigma_i^2} - \frac{|y - \mu_j|^2}{\sigma_j^2} \right) dy \\
&= \frac{1}{\pi^2 \sigma_i^2 \sigma_j^2} \exp \left(-\frac{\sigma_j^2 |\mu_i|^2 + \sigma_i^2 |\mu_j|^2}{\sigma_i^2 \sigma_j^2} \right) \\
&\quad \times \underbrace{\int_{y \in \mathbb{C}} \exp \left[-\left(\frac{1}{\sigma_i^2} + \frac{1}{\sigma_j^2} \right) |y|^2 + \frac{2}{\sigma_i^2} \text{Re}\{\mu_i^* y\} + \frac{2}{\sigma_j^2} \text{Re}\{\mu_j^* y\} \right] dy}_{Q},
\end{aligned} \tag{60}$$

where μ_i^* and μ_j^* are complex conjugate of μ_i and μ_j respectively. For the complex number y , by denoting the real component as y_R , and imaginary component y_I , the integration of Q is separated into real and imaginary parts

$$\begin{aligned}
Q &= \int_{-\infty}^{\infty} \exp \left(-\left(\frac{1}{\sigma_i^2} + \frac{1}{\sigma_j^2} \right) y_R^2 + 2 \left(\frac{\mu_{i,R}}{\sigma_i^2} + \frac{\mu_{j,R}}{\sigma_j^2} \right) y_R \right) dy_R \\
&\quad \times \int_{-\infty}^{\infty} \exp \left(-\left(\frac{1}{\sigma_i^2} + \frac{1}{\sigma_j^2} \right) y_I^2 + 2 \left(\frac{\mu_{i,I}}{\sigma_i^2} + \frac{\mu_{j,I}}{\sigma_j^2} \right) y_I \right) dy_I.
\end{aligned} \tag{61}$$

The integral (61) are computed using the following identity:

$$\int_{-\infty}^{\infty} \exp(-ay^2 + 2by) dy = \sqrt{\frac{\pi}{a}} \exp\left(\frac{b^2}{a}\right), \quad a > 0. \tag{62}$$

Then, Q is computed as

$$Q = \frac{\pi \sigma_i^2 \sigma_j^2}{\sigma_i^2 + \sigma_j^2} \exp \left(\frac{|\mu_i|^2 \sigma_j^4 + |\mu_j|^2 \sigma_i^4 + 2 \sigma_i^2 \sigma_j^2 (\mu_{i,R} \mu_{j,R} + \mu_{i,I} \mu_{j,I})}{\sigma_i^2 \sigma_j^2 (\sigma_i^2 + \sigma_j^2)} \right). \tag{63}$$

Using (60), (62), and (63) we have

$$\epsilon_{i,j} = \frac{1}{\pi(\sigma_i^2 + \sigma_j^2)} \exp \left(-\frac{|\mu_i - \mu_j|^2}{\sigma_i^2 + \sigma_j^2} \right). \tag{64}$$

Therefore, we obtain the lower bound of $H(Y)$ as

$$H(Y) \geq H_{\text{Low}}(Y) = - \sum_i w_i \log \sum_j w_j \epsilon_{i,j}. \quad (65)$$

Next, we compensate for the offset in asymptotic regimes as done in [31]. For this purpose, we limit ourselves to the case of $\gamma = 0.5$ and $\sigma_T^2 = 0$. Applying (65) gives a lower bound of mutual information as

$$\begin{aligned} I(X; Y) &\geq H_{\text{Low}}(Y) - H(Y|X) \\ &= -\log \left(\frac{\text{snr} + \text{snr} \exp \left(-\frac{\text{snr} |\mu_T|^2}{2} \right)}{4\pi} \right) - \log(\pi e / \text{snr}) \\ &= -\log \left(\frac{e}{4} \left(1 + \exp \left(-\frac{\text{snr} |\mu_T|^2}{2} \right) \right) \right) \\ &\triangleq I_{\text{Low}}(X; Y). \end{aligned} \quad (66)$$

Taking the limits to the two extreme SNR regimes gives the limiting values:

$$\begin{aligned} \lim_{\rho \rightarrow 0} I_{\text{Low}}(X; Y) &= \log(2/e), \\ \lim_{\rho \rightarrow \infty} I_{\text{Low}}(X; Y) &= \log(4/e). \end{aligned} \quad (67)$$

Notice that the distribution of Y is statistically equivalent to the received signal when sending a BPSK signal over an AWGN channel. Then, intuitively, the mutual information $I(X; Y)$ should approach to 0 when $\text{snr} = 0$, and to $\log 2$ when $\text{snr} = \infty$. Using these facts and two limiting values in (67), we can define the offset of approximation as

$$\Delta_{I(X; Y)} \triangleq I(X; Y) - I_{\text{Low}}(X; Y) = -\log(2/e). \quad (68)$$

Adding the offset (68) to (65) yields a tight approximation as

$$\begin{aligned} I(X; Y) &\approx H_{\text{Low}}(Y) + \Delta_{I(X; Y)} - H(Y|X) \\ &= - \sum_i w_i \log \sum_j w_j \epsilon_{i,j} - \log(2\pi / \text{snr}). \end{aligned} \quad (69)$$

Recall that the coefficients are $w_0 = 1 - \gamma$, $w_1 = \gamma$, $p_0(y) \sim \mathcal{CN}(0, 1/\text{snr})$, and $p_1(y) \sim \mathcal{CN}(\mu_T, \sigma_T^2 + (1/\text{snr}))$. By substituting these coefficients into (69), we have the following:

$$\begin{aligned}
I(X; Y) &\approx -(1 - \gamma) \log \left(\frac{\text{snr} (1 - \gamma)}{2\pi} + \frac{\text{snr} \gamma}{\pi(2 + \text{snr}\sigma_T^2)} e^{-\frac{\text{snr}|\mu_T|^2}{2 + \text{snr}\sigma_T^2}} \right) - \\
&\quad - \gamma \log \left(\frac{\text{snr} \gamma}{2\pi(1 + \text{snr}\sigma_T^2)} + \frac{\text{snr} (1 - \gamma)}{\pi(2 + \text{snr}\sigma_T^2)} e^{-\frac{\text{snr}|\mu_T|^2}{2 + \text{snr}\sigma_T^2}} \right) - \log \left(\frac{2\pi}{\text{snr}} \right) \\
&= \gamma \log(1 + \text{snr}\sigma_T^2) + H_b(\gamma) - (1 - \gamma) \log \left(1 + \frac{2\gamma}{(1 - \gamma)(2 + \text{snr}\sigma_T^2)} e^{-\frac{\text{snr}|\mu_T|^2}{2 + \text{snr}\sigma_T^2}} \right) \\
&\quad - \gamma \log \left(1 + \frac{2(1 - \gamma)(1 + \text{snr}\sigma_T^2)}{\gamma(2 + \text{snr}\sigma_T^2)} e^{-\frac{\text{snr}|\mu_T|^2}{2 + \text{snr}\sigma_T^2}} \right). \tag{70}
\end{aligned}$$

This completes the proof.

C. Proof of Theorem 5

Let $f_1(\lambda) = w_s \bar{R}_s(\lambda)$ and $f_2(\lambda) = w_c R_c(\lambda)$. First, we will show that both $f_1(\lambda)$ and $f_2(\lambda)$ are concave in $\lambda \in [0, 1]$. Then, satisfying (49) is sufficient to be the global optimal because $\bar{R}_{\text{sum}}(\lambda) = f_1(\lambda) + f_2(\lambda)$ is also concave. When there is no such $\bar{\lambda}^*$, the selection rule according to (50) is trivially obtained because i) $\frac{d\bar{R}_{\text{sum}}(\lambda)}{d\lambda} > 0$ implies that increasing λ from 0 to 1 increases $\bar{R}_{\text{sum}}(\lambda)$ and ii) $\frac{d\bar{R}_{\text{sum}}(\lambda)}{d\lambda} < 0$ implies that decreasing λ from 1 to 0 increases $\bar{R}_{\text{sum}}(\lambda)$. Therefore, the remaining task is to prove that $f_1(\lambda)$ and $f_2(\lambda)$ are concave in $\lambda \in [0, 1]$ by showing that the second order derivative is negative.

First, we consider $f_1(\lambda)$. Recall that $\bar{R}_s(\lambda) = \lambda B R_{n,k}(\bar{\text{snr}}_s(\lambda))$ and $\bar{\text{snr}}_s(\lambda) = \rho_{N-1}/\lambda$. We use the following I-MMSE relationship to derive the derivative expression:

$$\frac{dR_{n,k}(\bar{\text{snr}}_s(\lambda))}{d\bar{\text{snr}}_s(\lambda)} = \text{mmse}_{n,k}(\bar{\text{snr}}_s(\lambda)) \log_2 e. \tag{71}$$

Then, the first-order derivative of $f_1(\lambda)$ is given by

$$\begin{aligned}
\frac{df_1(\lambda)}{d\lambda} &= w_s B \left(R_{n,k}(\bar{\text{snr}}_s(\lambda)) - \bar{\text{snr}}_s(\lambda) \cdot \frac{dR_{n,k}(\bar{\text{snr}}_s(\lambda))}{d\bar{\text{snr}}_s(\lambda)} \right) \\
&= w_s B (R_{n,k}(\bar{\text{snr}}_s(\lambda)) - \bar{\text{snr}}_s(\lambda) \cdot \text{mmse}_{n,k}(\bar{\text{snr}}_s(\lambda)) \log_2 e) \geq 0, \tag{72}
\end{aligned}$$

where $\text{mmse}_{n,k}$ is in (23). Also, the non-negativeness come from the I-MMSE relationship in [29, Corollary 2]. The second-order derivative is given by

$$\frac{d^2 f_1(\lambda)}{d\lambda^2} = \frac{w_s (\bar{\text{snr}}_s(\lambda))^2}{\lambda} \cdot \frac{d \text{mmse}_{n,k}(\bar{\rho}(\lambda))}{d\bar{\text{snr}}_s(\lambda)} \log_2 e < 0. \tag{73}$$

Here, the inequality comes from the fact that MMSE is decreasing function of $\overline{\text{snr}}_r(\lambda)$ [32].

Second, we consider $f_2(\lambda)$. The direct computation yields the following first and second order derivative:

$$\begin{aligned}\frac{df_2(\lambda)}{d\lambda} &= -w_c B \log_2 \left(1 + \frac{\rho_c}{1-\lambda} \right) + \frac{w_c B \rho_c}{1-\lambda + \rho_c} \log_2 e < 0, \\ \frac{d^2 f_2(\lambda)}{d\lambda^2} &= -\frac{w_c B \rho_c^2}{(1-\lambda)(1-\lambda + \rho_c)^2} \log_2 e < 0.\end{aligned}\tag{74}$$

Because of (73) and (74), both $f_1(\lambda)$ and $f_2(\lambda)$ are concave in $\lambda \in [0, 1]$.

REFERENCES

- [1] J. A. Zhang, F. Liu, C. Masouros, R. W. Heath, Z. Feng, L. Zheng, and A. Petropulu, "An overview of signal processing techniques for joint communication and radar sensing," *IEEE J. Sel. Topics Signal Process.*, vol. 15, no. 6, pp. 1295–1315, Nov. 2021.
- [2] Y. Cui, F. Liu, X. Jing, and J. Mu, "Integrating sensing and communications for ubiquitous IoT: Applications, trends, and challenges," *IEEE Netw.*, vol. 35, no. 5, pp. 158–167, Sep. 2021.
- [3] F. Liu, C. Masouros, A. P. Petropulu, H. Griffiths, and L. Hanzo, "Joint radar and communication design: Applications, state-of-the-art, and the road ahead," *IEEE Trans. Commun.*, vol. 68, no. 6, pp. 3834–3862, Jun. 2020.
- [4] K. V. Mishra, M. B. Shankar, V. Koivunen, B. Ottersten, and S. A. Vorobyov, "Toward millimeter-wave joint radar communications: A signal processing perspective," *IEEE Signal Process. Mag.*, vol. 36, no. 5, pp. 100–114, Sep. 2019.
- [5] L. Zheng, M. Lops, Y. C. Eldar, and X. Wang, "Radar and communication coexistence: An overview: A review of recent methods," *IEEE Signal Process. Mag.*, vol. 36, no. 5, pp. 85–99, Sep. 2019.
- [6] D. Ma, N. Shlezinger, T. Huang, Y. Liu, and Y. C. Eldar, "Joint radar-communication strategies for autonomous vehicles: Combining two key automotive technologies," *IEEE Signal Process. Mag.*, vol. 37, no. 4, pp. 85–97, Jul. 2020.
- [7] P. Kumari, D. H. N. Nguyen, and R. W. Heath, "Performance trade-off in an adaptive IEEE 802.11ad waveform design for a joint automotive radar and communication system," in *Proc. IEEE Int. Conf. Acoustic Speech Signal Processing (ICASSP)*, Mar. 2017, pp. 4281–4285.
- [8] G. Wang, Y. Zou, Z. Zhou, K. Wu, and L. M. Ni, "We can hear you with Wi-Fi!" *IEEE Trans. Mobile Comput.*, vol. 15, no. 11, pp. 2907–2920, Nov. 2016.
- [9] F. Colone, D. Pastina, P. Falcone, and P. Lombardo, "WiFi-based passive ISAR for high-resolution cross-range profiling of moving targets," *IEEE Trans. Geosci. Remote Sens.*, vol. 52, no. 6, pp. 3486–3501, Jun. 2014.
- [10] R. Sankar, S. P. Chepuri, and Y. C. Eldar, "Beamforming in integrated sensing and communication systems with reconfigurable intelligent surfaces," *arXiv preprint arXiv:2206.07679*, 2022.
- [11] X. Liu, T. Huang, Y. Liu, and Y. C. Eldar, "Transmit beamforming with fixed covariance for integrated MIMO radar and multiuser communications," in *Proc. IEEE Int. Conf. Acoustic Speech Signal Processing (ICASSP)*, May 2022, pp. 8732–8736.
- [12] C. E. Shannon, "A mathematical theory of communication," *Bell System Technical Journal*, vol. 27, no. 3, pp. 379–423, Jul. 1948.
- [13] M. A. Richards, J. Scheer, and W. A. Holm, *Principles of Modern Radar: Basic Principles*. New York, NY, USA: Scitech, 2010.

- [14] H. V. Poor, *An Introduction to Signal Detection and Estimation*. New York: Springer-Verlag, 1994.
- [15] A. R. Chiriyath, B. Paul, G. M. Jacyna, and D. W. Bliss, "Inner bounds on performance of radar and communications co-existence," *IEEE Trans. Signal Process.*, vol. 64, no. 2, pp. 464–474, Jan. 2016.
- [16] B. Paul and D. W. Bliss, "Extending joint radar-communications bounds for FMCW radar with Doppler estimation," in *Proc. IEEE Radar Conf.*, May 2015, pp. 89–94.
- [17] A. R. Chiriyath, B. Paul, and D. W. Bliss, "Radar-communications convergence: Coexistence, cooperation, and co-design," *IEEE Trans. Cogn. Commun. Netw.*, vol. 3, no. 1, pp. 1–12, Mar. 2017.
- [18] Q. He, Z. Wang, J. Hu, and R. S. Blum, "Performance gains from cooperative MIMO radar and MIMO communication systems," *IEEE Signal Process. Lett.*, vol. 26, no. 1, pp. 194–198, Nov. 2018.
- [19] Y. Xiong, F. Liu, Y. Cui, W. Yuan, and T. X. Han, "Flowing the information from Shannon to Fisher: Towards the fundamental tradeoff in ISAC," *arXiv preprint arXiv:2204.06938*, 2022, [Online]. Available: <https://arxiv.org/abs/2204.06938>.
- [20] F. Liu, Y.-F. Liu, A. Li, C. Masouros, and Y. C. Eldar, "Cramér-Rao bound optimization for joint radar-communication beamforming," *IEEE Trans. Signal Process.*, vol. 70, pp. 240–253, Dec. 2021.
- [21] M. Kobayashi, G. Caire, and G. Kramer, "Joint state sensing and communication: Optimal tradeoff for a memoryless case," in *Proc. IEEE Int. Symp. Inf. Theory (ISIT)*, Jun. 2018, pp. 111–115.
- [22] M. Kobayashi, H. Hamad, G. Kramer, and G. Caire, "Joint state sensing and communication over memoryless multiple access channels," in *Proc. IEEE Int. Symp. Inf. Theory (ISIT)*, Jul. 2019, pp. 270–274.
- [23] M. Ahmadipour, M. Wigger, and M. Kobayashi, "Joint sensing and communication over memoryless broadcast channels," in *Proc. IEEE Inf. Theory Workshop (ITW)*, Apr. 2021, pp. 1–5.
- [24] H. Joudeh and F. M. Willems, "Joint communication and binary state detection," *IEEE J. Sel. Areas Inf. Theory*, vol. 3, no. 1, pp. 113–124, Mar. 2022.
- [25] K. V. Mishra and Y. C. Eldar, "Sub-nyquist radar: Principles and prototypes," in *Compressed sensing in radar signal processing*, A. Maio and A. Haimovich, Eds. Cambridge University Press, 2019.
- [26] M. A. Herman and T. Strohmer, "High-resolution radar via compressed sensing," *IEEE Trans. Signal Process.*, vol. 57, no. 6, pp. 2275–2284, Jun. 2009.
- [27] W. U. Bajwa, K. Gedalyahu, and Y. C. Eldar, "Identification of parametric underspread linear systems and super-resolution radar," *IEEE Trans. Signal Process.*, vol. 59, no. 6, pp. 2548–2561, Feb. 2011.
- [28] P. Swerling, "Probability of detection for fluctuating targets," *IRE Trans. Inf. Theory*, vol. 6, no. 2, pp. 269–308, Apr. 1960.
- [29] D. Guo, S. Shamai, and S. Verdú, "Mutual information and minimum mean-square error in Gaussian channels," *IEEE Trans. Inf. Theory*, vol. 51, no. 4, pp. 1261–1282, Apr. 2005.
- [30] A. Kolchinsky and B. D. Tracey, "Estimating mixture entropy with pairwise distances," *Entropy*, vol. 19, no. 7, p. 361, 2017.
- [31] J. Choi, Y. Nam, and N. Lee, "Spatial lattice modulation for MIMO systems," *IEEE Trans. Signal Process.*, vol. 66, no. 12, pp. 3185–3198, Apr. 2018.
- [32] D. Guo, Y. Wu, S. S. Shitz, and S. Verdú, "Estimation in Gaussian noise: Properties of the minimum mean-square error," *IEEE Trans. Inf. Theory*, vol. 57, no. 4, pp. 2371–2385, Apr. 2011.